Variable Actuation Modes in Parallel Manipulators: Impact on the Stiffness Behavior

Alexandr Klimchik
Center for Technologies in Robotics and Mechatronics Components
Innopolis University
Innopolis, Russia
a.klimchik@innopolis.ru

Anatol Pashkevich
Automation, Production and Computer Sciences
IMT Atlantique
Nantes, France
anatol.pashkevich@imt-atlantique.fr

Damien Chablat
LS2N
Centre National de la Recherche Scientifique
Nantes, France
damien.chablat@cnrs.fr

***Abstract*—The paper deals with the analysis of the manipulator actuation mode on the manipulator stiffness behavior. The main scientific contribution of the paper related to advancement of Matrix Structural Analysis (MSA) technique for the case of complex open-loop and closed-loop manipulators. The proposed approach presents the manipulator stiffness model as a homogeneous set of matrix equations describing the link properties that are complemented by a set of constraints describing connections between links that are presented in a similar way as link models. The proposed approach straightforwardly aggregates the stiffness model equations avoiding merging of columns and rows usually used in conventional MSA approach. The efficiency of this approach is illustrated by comparison analysis of NaVaRo manipulator for different actuation modes.**

I. Introduction

The manipulator stiffness analysis is one of the most important issues in design of robot mechanics for many industrial applications where the manipulators are subject to essential external loadings [1]. It allows designer to achieve required balance between the robot dynamics and positioning accuracy and to compensate relevant compliance errors using on-line or off-line error compensation technique [2-4]. For the stiffness modeling, there exist three main techniques [5], which are the Finite Element Analysis (FEA) [6-8], the Matrix Structural Analysis (MSA) [9-11] and the Virtual Joint Modeling (VJM) [12-15]. The most accurate but computationally expansive is the FEA [6], while the MSA is considered as a compromise technique, which operates with rather large elements such as flexible links connected by the actuated and passive joints in the overall manipulator structure. This obviously leads to the reduction of the computational expenses, but it requires some non-trivial actions for the MSA-based stiffness model generation that are proposed below.

Some reviews of existing works on manipulator stiffness analysis can be found in [16], [17], that cover results starting from the early works of Salisbury and Gosselin [18], [19] till recent years. Among latest contributions devoted to the MSA it worth mentioning the work of Cammarata [20], who introduced the notion of the Condensed Stiffness Matrix. Another useful extension of the MSA for the case of non-linear links/joints stiffness properties was proposed in [21] where a passive revolute joint was described by a rank-deficient force-dependent stiffness matrix. There are several works that deal with the MSA application to the stiffness analysis of particular manipulators. In [22] the MSA method was applied to EAST articulated maintenance arm with 11 degrees of freedoms, which is used for remote inspection of inner components inside the vacuum vessel. In [23] the MSA technique was employed to obtain a dynamic model of the industrial machining robot ABB IRB 6660 in order to predict vibration instability in machining. In [24] the MSA was applied to derive the static stiffness model of 9-dof redundant reconfigurable 3×PPPRS parallel manipulator for meso-Milling Machine Tool.

To our knowledge, the most essential contribution to the robot-oriented modification of the MSA was done by Deblase et. all [11] who proposed a general technique for taking into account passive joints and rigid connections. Nevertheless, some manual procedures of merging matrix components were not avoided, as well as preloadings and elastic connections were not treated. For this reason, this paper focuses on some enhancement of the MSA technique and its application to the stiffness analysis of the parallel manipulator NaVaRo [25].

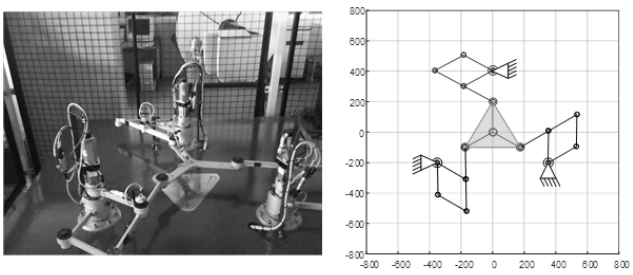

(a) robot NaVaRo (b) geometry of NaVaRo robot

Fig. 1. NaVaRo robot and its kinematics

II. Manipulator architecture

The NaVaRo robot (Fig 1) is a three-degree-of-freedom planar parallel manipulator with variable actuation schemes. It is composed of three identical legs and a moving platform formed of three segments rigidly linked at the central point. Each leg consists of four non-rigid links connected by five revolute joints to create a parallelogram linkage. Among them, there are four passive joints and one actuated joint connected to the motor via a double-clutching mechanism allowing to actuate one of two links adjacent to the motor axis. The latter determines the main particularity of the NaVARo robot that has

eight actuation modes that are switched to avoid kinematic singularities.

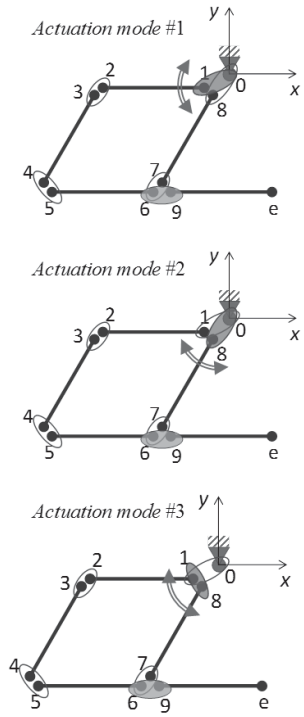

Fig. 2. MSA-based representation of the NaVaRo leg

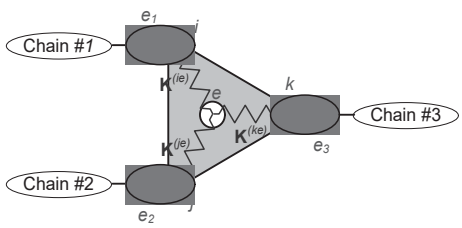

Fig. 3. MSA-based representation of the NaVaRo platform

To apply the MSA technique, let us split the mechanism into four parts: three kinematically identical legs and a mobile platform. For convenience, let us divide the longest link of the leg into two rigidly connected parts. This allows us to present each leg (Fig. 2) as a set of five flexible links (1,2), (3,4), (5,6), (7,8), (9,e) with passive connections of the nodes <2,3>, <4,5>, <6,7> and rigid connection of the nodes <6,9>. Depending on the actuation mode, the motor/clutch mechanics is specified as the passive connection of the nodes <0,8> and elastic connection of the nodes <0,1>, elastic connection of the nodes <0,8> and passive connection of the nodes <0,1> or passive connection of the nodes <0,1> and elastic connection of the nodes <1,8>. Besides, the moving platform can be presented as a mechanical structure composed of three flexible links (Fig. 3), which are rigidly connected to the end-effector on the right-hand side and to the manipulator's legs via a passive joint on the left-hand side.

III. Manipulator stiffness parameters

There exist several methods to obtain the stiffness matrix of a manipulator link. The most common and easier of them approximates the link by a simple beam, for which the stiffness matrix can be computed analytically using beam link, cross-section and material properties. The more accurate approach deals with multi-beam approximation where each link is presented via a serial chain of rigid bodies of regular shapes separated by several virtual springs. In this case, the link stiffness matrix can be obtained using a common procedure used in stiffness modelling of serial robots. However, even the second approach can be hardly applied to manipulator links with non-homogeneous structure and of complex shape with non-constant cross-section. It was shown before that for some complex-shape links four-beam approximation may give some components of the stiffness matrix twice differ from the real ones [26]. To achieve high accuracy of stiffness matrix components, the FEA-based identification procedure that was previously introduced in [8], [26]. The corresponding *algorithm* is schematically presented in Fig. 4.

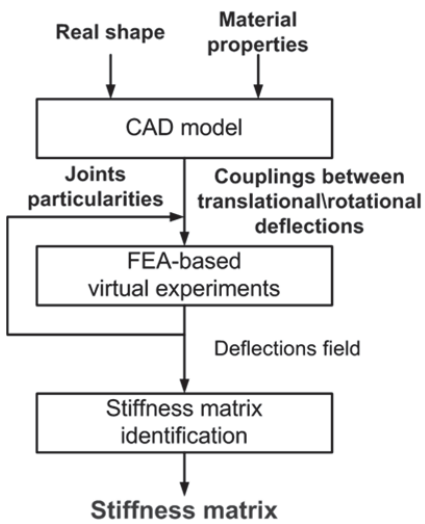

Fig. 4. Algorithm for stiffness matrix identification procedure

To achieve sophisticated model the stiffness parameters of the NaVaRo manipulator links were estimated using CAD-based technique and relevant data processing tools presented in details in [8]. To find them, the virtual forces/torques were applied to all links separately and corresponding deflections were obtained via the FEA modeling. These data were used for the identification of the link compliance coefficients. The obtained values are given in Table I, where the $\mathbf{C}_{22}^{(ij)}$ corresponds to the inverse of the stiffness matrix $\mathbf{K}_{22}^{(ij)}$. The stiffness coefficient of the actuator was estimated as $1.00 \cdot 10^4\ Nm/rad$.

The above presented identification technique allows us to obtain stiffness matrices of size 6×6. These matrices describe the link stiffness behavior that is evaluated assuming that one of the link ends is fixed and the loading is applied to the second one (Fig. 5a). However, the MSA-modeling operates

TABLE I. COMPLIANCE MATRICES OF THE NAVARO MANIPULATOR LINKS

Link	Compliance matrix $\mathbf{C}_{22}^{(ij)}$
Link (1,2) 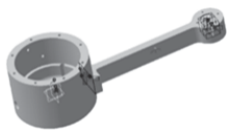	$\begin{bmatrix} 1.16\cdot10^{-8} & 0 & 0 & 0 & 0 & 0 \\ 0 & 9.21\cdot10^{-6} & 0 & 0 & 0 & 8.66\cdot10^{-5} \\ 0 & 0 & 2.32\cdot10^{-6} & 0 & -1.90\cdot10^{-5} & 0 \\ 0 & 0 & 0 & 8.67\cdot10^{-4} & 0 & 0 \\ 0 & 0 & -1.90\cdot10^{-5} & 0 & 2.00\cdot10^{-4} & 0 \\ 0 & 8.66\cdot10^{-5} & 0 & 0 & 0 & 9.90\cdot10^{-4} \end{bmatrix}$
Link (3.4)	$\begin{bmatrix} 1.10\cdot10^{-8} & 0 & 0 & 0 & 0 & 0 \\ 0 & 1.68\cdot10^{-5} & 0 & 0 & 0 & 1.30\cdot10^{-4} \\ 0 & 0 & 3.20\cdot10^{-6} & 0 & -2.40\cdot10^{-5} & 0 \\ 0 & 0 & 0 & 1.10\cdot10^{-3} & 0 & 0 \\ 0 & 0 & -2.40\cdot10^{-5} & 0 & 2.28\cdot10^{-4} & 0 \\ 0 & 1.30\cdot10^{-4} & 0 & 0 & 0 & 1.24\cdot10^{-3} \end{bmatrix}$
Link (5,6) 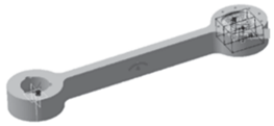	$\begin{bmatrix} 1.00\cdot10^{-8} & 0 & 0 & 0 & 0 & 0 \\ 0 & 1.78\cdot10^{-5} & 0 & 0 & 0 & 1.18\cdot10^{-4} \\ 0 & 0 & 2.85\cdot10^{-6} & 0 & -2.20\cdot10^{-5} & 0 \\ 0 & 0 & 0 & 9.93\cdot10^{-4} & 0 & 0 \\ 0 & 0 & -2.20\cdot10^{-5} & 0 & 2.10\cdot10^{-4} & 0 \\ 0 & 1.18\cdot10^{-4} & 0 & 0 & 0 & 1.13\cdot10^{-3} \end{bmatrix}$
Link (7,8)	$\begin{bmatrix} 1.01\cdot10^{-8} & 0 & 0 & 0 & 0 & 0 \\ 0 & 1.09\cdot10^{-5} & 0 & 0 & 0 & 9.61\cdot10^{-5} \\ 0 & 0 & 2.65\cdot10^{-6} & 0 & -2.12\cdot10^{-5} & 0 \\ 0 & 0 & 0 & 8.99\cdot10^{-4} & 0 & 0 \\ 0 & 0 & -2.12\cdot10^{-5} & 0 & 2.10\cdot10^{-4} & 0 \\ 0 & 9.61\cdot10^{-5} & 0 & 0 & 0 & 1.01\cdot10^{-3} \end{bmatrix}$
Link (9,*e*)	$\begin{bmatrix} 1.05\cdot10^{-8} & 0 & 0 & 0 & 0 & 0 \\ 0 & 1.68\cdot10^{-5} & 0 & 0 & 0 & 1.29\cdot10^{-4} \\ 0 & 0 & 3.21\cdot10^{-6} & 0 & -2.39\cdot10^{-5} & 0 \\ 0 & 0 & 0 & 1.05\cdot10^{-3} & 0 & 0 \\ 0 & 0 & -2.39\cdot10^{-5} & 0 & 2.20\cdot10^{-4} & 0 \\ 0 & 1.29\cdot10^{-4} & 0 & 0 & 0 & 1.18\cdot10^{-3} \end{bmatrix}$
Link (*i*,*e*)	$\begin{bmatrix} 7.66\cdot10^{-9} & 0 & 0 & 0 & 0 & 0 \\ 0 & 1.36\cdot10^{-6} & 0 & 0 & 0 & 8.42\cdot10^{-6} \\ 0 & 0 & 1.12\cdot10^{-5} & 0 & -8.48\cdot10^{-5} & 0 \\ 0 & 0 & 0 & 6.58\cdot10^{-4} & 0 & 0 \\ 0 & 0 & -8.48\cdot10^{-5} & 0 & 8.51\cdot10^{-4} & 0 \\ 0 & 8.42\cdot10^{-6} & 0 & 0 & 0 & 7.09\cdot10^{-5} \end{bmatrix}$

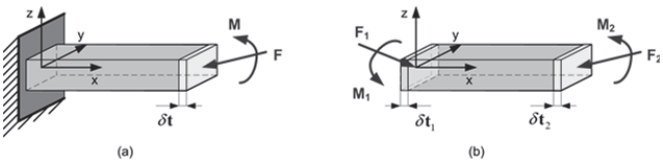

Fig. 5. Physical models of cantilever beam (a) and "free-free" beam (b)

with 12×12 stiffness matrices, which does not assume that any of the link ends is fixed. In contrast, it is assumed here that the links are subject to double-side loading and deflections are defined for both of this sides (Fig 5b). For such arrangement, the stiffness matrix should have size 12×12 because it defines the linear relations between two deflection vectors (of size 6 each) and two vectors of loading (of size 6 each). From a physical point of view, it is clear that both stiffness matrices (of size 6×6 and 12×12) describe the same properties of the link, while the smaller one contains exhaustive information on the stiffness. Hence, it is useful to obtain expressions that allow us to transform a 6×6 stiffness matrix into a 12×12 one, which is required for the MSA-modeling technique [27].

To derive desired expressions, let us denote the above described stiffness matrices as $\mathbf{K}_{6\times6}$ and $\mathbf{K}_{12\times12}$. Let us also assume that the link geometry and its spatial location are defined by the vector $\mathbf{L}=(l_x, l_y, l_z)^{\mathrm{T}}$ connecting corresponding nodes. Besides considering that both of the matrices are symmetrical, it is convenient to present them in the block form as

$$\mathbf{K}_{6\times6}=\begin{bmatrix}\mathbf{K}_a & \mathbf{K}_b\\ \mathbf{K}_c & \mathbf{K}_d\end{bmatrix} \qquad \mathbf{K}_c=\mathbf{K}_b^{\mathrm{T}} \tag{1}$$

$$\mathbf{K}_{12\times 12}=\begin{bmatrix}\mathbf{K}_{11} & \mathbf{K}_{12}\\ \mathbf{K}_{21} & \mathbf{K}_{22}\end{bmatrix},\quad \mathbf{K}_{21}=\mathbf{K}_{12}{}^{\mathrm{T}},$$
$$\mathbf{K}_{ij}=\begin{bmatrix}\mathbf{K}_{ija} & \mathbf{K}_{ijb}\\ \mathbf{K}_{ijc} & \mathbf{K}_{ijd}\end{bmatrix}\quad \mathbf{K}_{ijc}=\mathbf{K}_{ijb}{}^{\mathrm{T}} \tag{2}$$

where $i=1,2$ and $j=1,2$.

Let us consider simultaneously two static equilibriums

$$\begin{bmatrix}\mathbf{F}\\ \mathbf{M}\end{bmatrix}=\begin{bmatrix}\mathbf{K}_a & \mathbf{K}_b\\ \mathbf{K}_c & \mathbf{K}_d\end{bmatrix}\cdot\begin{bmatrix}\delta\mathbf{p}\\ \delta\boldsymbol{\varphi}\end{bmatrix} \tag{3}$$

$$\begin{bmatrix}\mathbf{W}_1\\ \mathbf{W}_2\end{bmatrix}=\begin{bmatrix}\mathbf{K}_{11} & \mathbf{K}_{12}\\ \mathbf{K}_{21} & \mathbf{K}_{22}\end{bmatrix}\cdot\begin{bmatrix}\delta\mathbf{t}_1\\ \delta\mathbf{t}_2\end{bmatrix} \tag{4}$$

where the first one corresponds to the single-side loading (cantilever beam) and the second equation corresponds to the double-side loading. Here, for the single-side loading case, $\mathbf{F}$ and $\mathbf{M}$ are the force and torque applied to the non-fixed link end, $\delta\mathbf{p}$ and $\delta\boldsymbol{\varphi}$ are translational and rotational deflections caused by external loading. Similarly, for the double-side loading case, $\mathbf{W}_1=(\mathbf{F}_1,\mathbf{M}_1)^{\mathrm{T}}$ and $\mathbf{W}_2=(\mathbf{F}_2,\mathbf{M}_2)^{\mathrm{T}}$ are the wrenches applied to the link ends, $\delta\mathbf{t}_1$ and $\delta\mathbf{t}_2$ are the deflections of corresponding link ends under the loadings $\mathbf{W}_1$ and $\mathbf{W}_2$. It is obvious that in both cases the model variables should satisfy the static equilibrium conditions, which eliminate some redundancy in notations for the second case.

To obtain desired matrices, let us assume first that for the double-side model $\delta\mathbf{t}_1=\mathbf{0}$. This allows us straightforwardly apply equation (3) and static equilibrium constrain that yield

$$\mathbf{W}_1=\begin{bmatrix}-\mathbf{F}\\ -\mathbf{M}+\mathbf{F}\times\mathbf{L}\end{bmatrix};\quad \mathbf{W}_2=\begin{bmatrix}\mathbf{F}\\ \mathbf{M}\end{bmatrix};\quad \delta\mathbf{t}_2=\begin{bmatrix}\delta\mathbf{t}\\ \delta\boldsymbol{\varphi}\end{bmatrix} \tag{5}$$

that leads to the following presentation of equation (4)

$$\begin{bmatrix}-\mathbf{F}\\ -\mathbf{M}+\mathbf{F}\times\mathbf{L}\\ \mathbf{F}\\ \mathbf{M}\end{bmatrix}=\begin{bmatrix}\mathbf{K}_{11} & \mathbf{K}_{12}\\ \mathbf{K}_{21} & \mathbf{K}_{22}\end{bmatrix}\cdot\begin{bmatrix}\mathbf{0}\\ \mathbf{0}\\ \delta\mathbf{p}\\ \delta\boldsymbol{\varphi}\end{bmatrix} \tag{6}$$

which leads to

$$\mathbf{K}_{22}=\mathbf{K}_{6\times 6} \tag{7}$$

Further, considering that $\mathbf{F}\times\mathbf{L}=-(\mathbf{L}\times)\cdot\mathbf{F}$ and using symmetrical properties of stiffness matrix,

$$\mathbf{K}_{12}=\begin{bmatrix}-\mathbf{K}_a & -\mathbf{K}_b\\ -\mathbf{K}_c-[\mathbf{L}\times]\cdot\mathbf{K}_a & -\mathbf{K}_d-[\mathbf{L}\times]\cdot\mathbf{K}_b\end{bmatrix};$$
$$\mathbf{K}_{21}=\mathbf{K}_{12}^{\mathrm{T}}=\begin{bmatrix}-\mathbf{K}_a & -\mathbf{K}_b+\mathbf{K}_a\cdot[\mathbf{L}\times]\\ -\mathbf{K}_c & -\mathbf{K}_d+\mathbf{K}_c\cdot[\mathbf{L}\times]\end{bmatrix} \tag{8}$$

where $[\mathbf{L}\times]$ denotes the 3×3 skew-symmetric matrix derived from the vector $\mathbf{L}$

Similarly, assuming that $\delta\mathbf{t}_2=\mathbf{0}$, the model (4) can be re-written using expressions

$$\mathbf{W}_1=\begin{bmatrix}\mathbf{F}\\ \mathbf{M}\end{bmatrix};\quad \mathbf{W}_2=\begin{bmatrix}-\mathbf{F}\\ -\mathbf{M}+\mathbf{F}\times\mathbf{L}\end{bmatrix};\quad \delta\mathbf{t}_1=\begin{bmatrix}\delta\mathbf{t}\\ \delta\boldsymbol{\varphi}\end{bmatrix} \tag{9}$$

and presented in the form

$$\begin{bmatrix}\mathbf{F}\\ \mathbf{M}\\ -\mathbf{F}\\ -\mathbf{M}+\mathbf{F}\times\mathbf{L}\end{bmatrix}=\begin{bmatrix}\mathbf{K}_{11} & \mathbf{K}_{12}\\ \mathbf{K}_{21} & \mathbf{K}_{22}\end{bmatrix}\cdot\begin{bmatrix}\delta\mathbf{p}_1\\ \delta\boldsymbol{\varphi}_1\\ \mathbf{0}\\ \mathbf{0}\end{bmatrix} \tag{10}$$

that after substitution of $\mathbf{K}_{12}$, $\mathbf{K}_{21}$, $\mathbf{K}_{22}$ and relevant transformations gives the following expression

$$\mathbf{K}_{11}=\begin{bmatrix}\mathbf{K}_a & \mathbf{K}_b-\mathbf{K}_a\cdot[\mathbf{L}\times]\\ \mathbf{K}_c+[\mathbf{L}\times]\cdot\mathbf{K}_a & \mathbf{K}_d-\mathbf{K}_c\cdot[\mathbf{L}\times]+[\mathbf{L}\times]\cdot\mathbf{K}_b-\\ & -[\mathbf{L}\times]\cdot\mathbf{K}_a\cdot[\mathbf{L}\times]\end{bmatrix} \tag{11}$$

Therefore, the stiffness matrix identification technique presented before can also produce 12×12 matrices required for the manipulator stiffness modeling using the MSA-approach.

It is clear that in general case when the link is arbitrary oriented with respect to the global coordinate system, the above equations should be slightly modified by simply rotating the local stiffness matrices

$$\begin{bmatrix}\mathbf{K}_{11}^g & \mathbf{K}_{12}^g\\ \mathbf{K}_{21}^g & \mathbf{K}_{22}^g\end{bmatrix}=\begin{bmatrix}\mathbf{Q}\cdot\mathbf{K}_{11}\cdot\mathbf{Q}^T & \mathbf{Q}\cdot\mathbf{K}_{12}\cdot\mathbf{Q}^T\\ \mathbf{Q}\cdot\mathbf{K}_{21}\cdot\mathbf{Q}^T & \mathbf{Q}\cdot\mathbf{K}_{22}\cdot\mathbf{Q}^T\end{bmatrix} \tag{12}$$

where $\mathbf{Q}=diag(\mathbf{R},\mathbf{R})$ is composed of two similar orthogonal matrices $\mathbf{R}$ defining the orientation of the local coordinate system of the link (*ij*) relative to the global one and left superscript "*g*" indicates that matrix is presented in the global coordinate system that will for simplicity purpose will be omitted further (since all matrices assumed to be computed in a global coordinate system).

IV. Aggregated Stiffness Model

The MSA equations for robotic manipulator are derived from three main sources: (i) link models, (ii) joint models and (iii) boundary conditions. The first of them describes the force-displacement relations for all links. The second group of equations ensures the displacement compatibility and force/torque equilibrium for each internal connection. The third group of equations is issued from the manipulator connections to the environment.

In the general form, the aggregated stiffness model can be presented as follows

$$\begin{bmatrix}\mathbf{A}_{\mathrm{W}}^{(1)} & \mathbf{A}_{\Delta\mathrm{t}}^{(1)}\\ \mathbf{A}_{\mathrm{W}}^{(2)} & \mathbf{A}_{\Delta\mathrm{t}}^{(2)}\\ \cdots & \cdots\end{bmatrix}\cdot\begin{bmatrix}\{\mathbf{W}_i\}\\ \{\Delta\mathbf{t}_i\}\end{bmatrix}=\begin{bmatrix}\mathbf{b}_0^{(1)}\\ \mathbf{b}_0^{(2)}\\ \cdots\end{bmatrix} \tag{13}$$

where $\mathbf{W}_i$ and $\Delta\mathbf{t}_i$ are the wrench and displacement of the ith node, while the matrices $\mathbf{A}_{\mathrm{W}}^{(i)}$, $\mathbf{A}_{\Delta\mathrm{t}}^{(i)}$ and the vectors $\mathbf{b}_0^{(i)}$ are defined below. Using notations adopted in [28, 29], the con-

tribution of the links, joints and constraints can be expressed in the following way,

∀ flexible links:

$$\left[\{-\mathbf{I}_{12\times12}\}\ \{\mathbf{K}^{ij}_{12\times12}\}\right]\cdot\begin{bmatrix}\{\mathbf{W}_i\}\\ \{\Delta\mathbf{t}_i\}\end{bmatrix}=\mathbf{0} \tag{14}$$

∀ rigid links:

$$\begin{bmatrix}\mathbf{0} & \{\mathbf{D}^{ij}_{6\times6},-\mathbf{I}_{6\times6}\}\\ \{\mathbf{I}_{6\times6},\mathbf{D}^{ij\,T}_{6\times6}\} & \mathbf{0}\end{bmatrix}\cdot\begin{bmatrix}\{\mathbf{W}_i\}\\ \{\Delta\mathbf{t}_i\}\end{bmatrix}=\begin{bmatrix}\mathbf{0}\\ \mathbf{0}\end{bmatrix} \tag{15}$$

for flexible platform:

$$\begin{bmatrix}\{-\mathbf{I}_{6\times6}\} & \{\mathbf{K}^{ij}_{6\times6}\}\\ \mathbf{0} & \{\mathbf{K}^{ij}_{6\times6}\}\end{bmatrix}\cdot\begin{bmatrix}\{\mathbf{W}_i\}\\ \{\Delta\mathbf{t}_i\}\end{bmatrix}=\begin{bmatrix}\mathbf{0}\\ \mathbf{W}_{ext}\end{bmatrix} \tag{16}$$

for rigid platform:

$$\begin{bmatrix}\mathbf{0} & \{-\mathbf{I}_{6\times6},\mathbf{D}^{(ei)}_{6\times6}\}\\ \{\mathbf{D}^{(ei)T}_{6\times6}\} & \mathbf{0}\end{bmatrix}\cdot\begin{bmatrix}\{\mathbf{W}_i\}\\ \{\Delta\mathbf{t}_i\}\end{bmatrix}=\begin{bmatrix}\mathbf{0}\\ \mathbf{W}_{ext}\end{bmatrix} \tag{17}$$

∀ rigid joints:

$$\begin{bmatrix}\mathbf{0} & \{\mathbf{I}_{6\times6},-\mathbf{I}_{6\times6}\}\\ \{\mathbf{I}_{6\times6},\mathbf{I}_{6\times6}\} & \mathbf{0}\end{bmatrix}\cdot\begin{bmatrix}\{\mathbf{W}_i\}\\ \{\Delta\mathbf{t}_i\}\end{bmatrix}=\begin{bmatrix}\mathbf{0}\\ \{\mathbf{W}^0_{ij}\}\end{bmatrix} \tag{18}$$

∀ passive joints:

$$\begin{bmatrix}\mathbf{0} & \{\mathbf{\Lambda}^r_{*ij},-\mathbf{\Lambda}^r_{*ij}\}\\ \{\mathbf{\Lambda}^r_{*ij},\mathbf{\Lambda}^r_{*ij}\} & \mathbf{0}\\ \{\mathbf{\Lambda}^p_{*ij}\} & \mathbf{0}\end{bmatrix}\cdot\begin{bmatrix}\{\mathbf{W}_i\}\\ \{\Delta\mathbf{t}_i\}\end{bmatrix}=\begin{bmatrix}\mathbf{0}\\ \{\mathbf{\Lambda}^r_{*ij}\mathbf{W}^0_{ij}\}\\ \mathbf{0}\end{bmatrix} \tag{19}$$

∀ elastic joints:

$$\begin{bmatrix}\mathbf{0} & \{\mathbf{\Lambda}^r_{*ij},-\mathbf{\Lambda}^r_{*ij}\}\\ \{\mathbf{I}_{6\times6},\mathbf{I}_{6\times6}\} & \mathbf{0}\\ \mathbf{\Lambda}^e_{*ij} & \{\mathbf{K}^e_{ij}\mathbf{\Lambda}^e_{*ij},-\mathbf{K}^e_{ij}\mathbf{\Lambda}^e_{*ij}\}\end{bmatrix}\cdot\begin{bmatrix}\{\mathbf{W}_i\}\\ \{\Delta\mathbf{t}_i\}\end{bmatrix}=\begin{bmatrix}\mathbf{0}\\ \{\mathbf{W}^0_{ij}\}\\ \{\mathbf{\Lambda}^e_{*ij}\mathbf{W}^0_{ij}\}\end{bmatrix} \tag{20}$$

∀ rigid supports:

$$\left[\mathbf{0}\ \{\mathbf{I}_{6\times6}\}\right]\cdot\begin{bmatrix}\{\mathbf{W}_i\}\\ \{\Delta\mathbf{t}_i\}\end{bmatrix}=\mathbf{0} \tag{21}$$

∀ passive supports:

$$\begin{bmatrix}\mathbf{0} & \{\mathbf{\Lambda}^r_{*ij}\}\\ \{\mathbf{\Lambda}^p_{*ij}\} & \mathbf{0}\end{bmatrix}\cdot\begin{bmatrix}\{\mathbf{W}_i\}\\ \{\Delta\mathbf{t}_i\}\end{bmatrix}=\begin{bmatrix}\mathbf{0}\\ \mathbf{0}\end{bmatrix} \tag{22}$$

∀ elastic supports:

$$\begin{bmatrix}\mathbf{0} & \{\mathbf{\Lambda}^r_{*ij}\}\\ \{\mathbf{\Lambda}^e_{*ij}\} & \{\mathbf{K}^e_{ij}\mathbf{\Lambda}^e_{*ij}\}\end{bmatrix}\cdot\begin{bmatrix}\{\mathbf{W}_i\}\\ \{\Delta\mathbf{t}_i\}\end{bmatrix}=\begin{bmatrix}\mathbf{0}\\ \{\mathbf{W}^0_{ij}\}\end{bmatrix} \tag{23}$$

∀ external loadings:

$$\left[\{-\mathbf{I}_{6\times6}\}\ \mathbf{0}\right]\cdot\begin{bmatrix}\{\mathbf{W}_i\}\\ \{\Delta\mathbf{t}_i\}\end{bmatrix}=\{\mathbf{W}^{ext}_i\} \tag{24}$$

For computational convenience, the equations (14)-(24) can be arranged in the aggregated linear matrix equation

$$\begin{bmatrix}\mathbf{S}_{agr} & \mathbf{K}_{agr}\\ \mathbf{E}_{agr} & \mathbf{F}_{agr}\end{bmatrix}\cdot\begin{bmatrix}\mathbf{W}_{agr}\\ \Delta\mathbf{t}_{agr}\end{bmatrix}=\begin{bmatrix}\mathbf{b}_{agr}\\ \mathbf{W}_{ext}\end{bmatrix} \tag{25}$$

where the matrices $\mathbf{S}_{agr}$, $\mathbf{K}_{agr}$, $\mathbf{E}_{agr}$, $\mathbf{F}_{agr}$, $\mathbf{b}_{agr}$, $\mathbf{W}_{ext}$ are generated using relevant link/joint models or boundary conditions, while the vectors $\mathbf{W}_{agr}$ and $\Delta\mathbf{t}_{agr}$ contain all variables describing the wrenches and displacements, respectively. To find the desired Cartesian stiffness matrix, let us divide the node displacement variables $\Delta\mathbf{t}_{agr}$ into two groups $\Delta\mathbf{t}_m$ and $\Delta\mathbf{t}_e$ corresponding to the manipulator internal nodes and the end-effector node, where the external wrench $\mathbf{W}_e$ is applied. The latter allows us to rewrite the system (25) in the form

$$\left[\begin{array}{cc|c}\mathbf{S}_{agr} & \mathbf{K}_m & \mathbf{K}_e\\ \mathbf{E}_m & \mathbf{F}_m & \mathbf{C}_e\\ \hline \mathbf{E}_e & \mathbf{F}_e & \mathbf{D}\end{array}\right]\cdot\left[\begin{array}{c}\mathbf{W}_{agr}\\ \Delta\mathbf{t}_m\\ \hline \Delta\mathbf{t}_e\end{array}\right]=\left[\begin{array}{c}\mathbf{b}_{agr}\\ \mathbf{W}_m\\ \hline \mathbf{W}_e\end{array}\right] \tag{26}$$

and further, present it as

$$\begin{bmatrix}\mathbf{A} & \mathbf{B}\\ \mathbf{C} & \mathbf{D}\end{bmatrix}\cdot\left[\begin{array}{c}\boldsymbol{\mu}\\ \hline \Delta\mathbf{t}_e\end{array}\right]=\left[\begin{array}{c}\mathbf{b}\\ \hline \mathbf{W}_e\end{array}\right] \tag{27}$$

where all internal variables are included in the vector $\boldsymbol{\mu}=col(\mathbf{W}_{agr},\Delta\mathbf{t}_m)$ and

$$\mathbf{A}=\begin{bmatrix}\mathbf{S}_{agr} & \mathbf{K}_m\\ \mathbf{E}_m & \mathbf{F}_m\end{bmatrix};\quad \mathbf{B}=\begin{bmatrix}\mathbf{K}_e\\ \mathbf{C}_e\end{bmatrix};\quad \mathbf{C}=\begin{bmatrix}\mathbf{E}_e & \mathbf{F}_e\end{bmatrix};\quad \mathbf{b}=\begin{bmatrix}\mathbf{b}_{agr}\\ \mathbf{W}_m\end{bmatrix} \tag{28}$$

Using the obtained system, the desired Cartesian stiffness matrix can be computed as

$$\mathbf{K}_C=\mathbf{D}-\mathbf{C}\cdot\mathbf{A}^{-1}\cdot\mathbf{B} \tag{29}$$

It is worth mentioning that $\mathbf{A}^{-1}$ usually exists while the aggregated matrix in (27) is rank deficient. Overall algorithm for stiffness behavior estimation using the MSA method summarized

Algorithm 1. Algorithm for stiffness behavior using MSA

Step #1. Define node points and type of connections between them.
Step #2. Identify stiffness model parameters using algorithm presented in Fig. 4.
Step #3. Compute 12×12 stiffness matrices using eq. (7), (8) and (11).
Step #4. Define manipulator configuration by solving direct/inverse kinematic problem.
Step #5. Compute rotation matrices **R** for all flexible links.
Step #6. Compute stiffness matrices for all flexible components in a global coordinate system (12).
Step #7. Write equations for flexible and rigid links/platforms using eq. (14)-(17).
Step #8. Write equations for rigid, passive and elastic joints using eq. (18)-(20).
Step #9. Write boundary constraints using eq. (21)-(24).
Step #10. Collect all matrix equations in a single system of eq. (13).
Step #11. Extract reference point deflection and corresponding external force using eq. (26).
Step #12. Compute Stiffness Matrix using eq. (29).
Step #13. Evaluate manipulator performance using desired metric.

V. STIFFNESS MODEL OF NAVARO MANIPULATOR

Using the developed technique, after assembling all equations describing the constraints and boundary conditions, the aggregated stiffness model of a single manipulator leg is presented as follows

$$\begin{bmatrix} -\mathbf{I}_{60\times60} & \mathbf{K}_{links} \\ \mathbf{0}_{31\times60} & \mathbf{A}_{agr} \\ \mathbf{B}_{agr} & \mathbf{0}_{22\times60} \\ \mathbf{C}_{agr} & \mathbf{D}_{agr} \\ \mathbf{E}_{agr} & \mathbf{F}_{6\times60} \end{bmatrix}_{120\times120} \cdot \begin{bmatrix} \mathbf{W}_{agr} \\ \Delta\mathbf{t}_{agr} \end{bmatrix}_{120\times1} = \begin{bmatrix} \mathbf{0}_{114\times1} \\ \mathbf{W}_e \end{bmatrix}_{120\times1} \tag{30}$$

where $\mathbf{K}_{links}$ aggregates all stiffness matrices of the flexible links and is the same for all actuation modes since mechanical properties remains the same. In contrast some other blocks depend on the actuation mode. To distinguish matrices for different actuation modes let us denote them by the superscripts '(1)', '(2)' or '(3)'. For the actuation mode (1) corresponding block matrices have the form

$$\mathbf{A}^{(1)}_{agr} = \left[\begin{array}{cc|cc|cc|cc|cc} 0 & \mathbf{\Lambda}^r_* & -\mathbf{\Lambda}^r_* & 0 & 0 & 0 & 0 & 0 & 0 & 0 \\ \hline 0 & 0 & 0 & \mathbf{\Lambda}^r_* & -\mathbf{\Lambda}^r_* & 0 & 0 & 0 & 0 & 0 \\ \hline 0 & 0 & 0 & 0 & 0 & \mathbf{\Lambda}^r_* & -\mathbf{\Lambda}^r_* & 0 & 0 & 0 \\ 0 & 0 & 0 & 0 & 0 & \mathbf{I} & 0 & 0 & -\mathbf{I} & 0 \\ \hline 0 & 0 & 0 & 0 & 0 & 0 & 0 & \mathbf{\Lambda}^r_* & 0 & 0 \\ \hline \mathbf{\Lambda}^r_* & 0 & 0 & 0 & 0 & 0 & 0 & 0 & 0 & 0 \end{array}\right]_{31\times60} \tag{31}$$

$$\mathbf{B}^{(1)}_{agr} = \left[\begin{array}{cc|cc|cc|cc|cc} 0 & \mathbf{\Lambda}^r_* & \mathbf{\Lambda}^r_* & 0 & 0 & 0 & 0 & 0 & 0 & 0 \\ 0 & \mathbf{\Lambda}^p_* & 0 & 0 & 0 & 0 & 0 & 0 & 0 & 0 \\ 0 & 0 & \mathbf{\Lambda}^p_* & 0 & 0 & 0 & 0 & 0 & 0 & 0 \\ \hline 0 & 0 & 0 & \mathbf{\Lambda}^r_* & \mathbf{\Lambda}^r_* & 0 & 0 & 0 & 0 & 0 \\ 0 & 0 & 0 & \mathbf{\Lambda}^p_* & 0 & 0 & 0 & 0 & 0 & 0 \\ 0 & 0 & 0 & 0 & \mathbf{\Lambda}^p_* & 0 & 0 & 0 & 0 & 0 \\ \hline 0 & 0 & 0 & 0 & 0 & \mathbf{\Lambda}^r_* & \mathbf{\Lambda}^r_* & 0 & \mathbf{\Lambda}^r_* & 0 \\ 0 & 0 & 0 & 0 & 0 & \mathbf{\Lambda}^p_* & 0 & 0 & \mathbf{\Lambda}^p_* & 0 \\ 0 & 0 & 0 & 0 & 0 & 0 & \mathbf{\Lambda}^p_* & 0 & 0 & 0 \\ \hline 0 & 0 & 0 & 0 & 0 & 0 & 0 & \mathbf{\Lambda}^p_* & 0 & 0 \end{array}\right]_{22\times60} \tag{32}$$

$$\mathbf{C}^{(1)}_{agr} = \left[\begin{array}{cc|cc|cc|cc|cc} -\mathbf{\Lambda}^e_* & 0 & 0 & 0 & 0 & 0 & 0 & 0 & 0 & 0 \end{array}\right]_{1\times60} \tag{33}$$

$$\mathbf{D}^{(1)}_{agr} = \left[\begin{array}{cc|cc|cc|cc|cc} K_e\mathbf{\Lambda}^e_* & 0 & 0 & 0 & 0 & 0 & 0 & 0 & 0 & 0 \end{array}\right]_{1\times60} \tag{34}$$

$$\mathbf{E}^{(1)}_{agr} = \left[\begin{array}{cc|cc|cc|cc|cc} 0 & 0 & 0 & 0 & 0 & 0 & 0 & 0 & 0 & \mathbf{I} \end{array}\right]_{6\times60} . \tag{35}$$

$$\mathbf{F}^{(1)}_{agr} = \left[\begin{array}{cc|cc|cc|cc|cc} 0 & 0 & 0 & 0 & 0 & 0 & 0 & 0 & 0 & 0 \end{array}\right]_{6\times60} \tag{36}$$

For the actuation mode (2) corresponding block matrices have the form

$$\mathbf{A}^{(2)}_{agr} = \left[\begin{array}{cc|cc|cc|cc|cc} 0 & \mathbf{\Lambda}^r_* & -\mathbf{\Lambda}^r_* & 0 & 0 & 0 & 0 & 0 & 0 & 0 \\ \hline 0 & 0 & 0 & \mathbf{\Lambda}^r_* & -\mathbf{\Lambda}^r_* & 0 & 0 & 0 & 0 & 0 \\ \hline 0 & 0 & 0 & 0 & 0 & \mathbf{\Lambda}^r_* & -\mathbf{\Lambda}^r_* & 0 & 0 & 0 \\ 0 & 0 & 0 & 0 & 0 & \mathbf{I} & 0 & 0 & -\mathbf{I} & 0 \\ \hline 0 & 0 & 0 & 0 & 0 & 0 & 0 & \mathbf{\Lambda}^r_* & 0 & 0 \\ \hline \mathbf{\Lambda}^r_* & 0 & 0 & 0 & 0 & 0 & 0 & 0 & 0 & 0 \end{array}\right]_{31\times60} \tag{37}$$

$$\mathbf{B}^{(2)}_{agr} = \left[\begin{array}{cc|cc|cc|cc|cc} 0 & \mathbf{\Lambda}^r_* & \mathbf{\Lambda}^r_* & 0 & 0 & 0 & 0 & 0 & 0 & 0 \\ 0 & \mathbf{\Lambda}^p_* & 0 & 0 & 0 & 0 & 0 & 0 & 0 & 0 \\ 0 & 0 & \mathbf{\Lambda}^p_* & 0 & 0 & 0 & 0 & 0 & 0 & 0 \\ \hline 0 & 0 & 0 & \mathbf{\Lambda}^r_* & \mathbf{\Lambda}^r_* & 0 & 0 & 0 & 0 & 0 \\ 0 & 0 & 0 & \mathbf{\Lambda}^p_* & 0 & 0 & 0 & 0 & 0 & 0 \\ 0 & 0 & 0 & 0 & \mathbf{\Lambda}^p_* & 0 & 0 & 0 & 0 & 0 \\ \hline 0 & 0 & 0 & 0 & 0 & \mathbf{\Lambda}^r_* & \mathbf{\Lambda}^r_* & 0 & \mathbf{\Lambda}^r_* & 0 \\ 0 & 0 & 0 & 0 & 0 & \mathbf{\Lambda}^p_* & 0 & 0 & \mathbf{\Lambda}^p_* & 0 \\ 0 & 0 & 0 & 0 & 0 & 0 & \mathbf{\Lambda}^p_* & 0 & 0 & 0 \\ \hline \mathbf{\Lambda}^p_* & 0 & 0 & 0 & 0 & 0 & 0 & 0 & 0 & 0 \end{array}\right]_{22\times60} \tag{38}$$

$$\mathbf{C}^{(2)}_{agr} = \left[\begin{array}{cc|cc|cc|cc|cc} 0 & 0 & 0 & 0 & 0 & 0 & 0 & -\mathbf{\Lambda}^e_* & 0 & 0 \end{array}\right]_{1\times60} \tag{39}$$

$$\mathbf{D}^{(2)}_{agr} = \left[\begin{array}{cc|cc|cc|cc|cc} 0 & 0 & 0 & 0 & 0 & 0 & 0 & K_e\mathbf{\Lambda}^e_* & 0 & 0 \end{array}\right]_{1\times60} \tag{40}$$

$$\mathbf{E}^{(2)}_{agr} = \left[\begin{array}{cc|cc|cc|cc|cc} 0 & 0 & 0 & 0 & 0 & 0 & 0 & 0 & 0 & \mathbf{I} \end{array}\right]_{6\times60} . \tag{41}$$

$$\mathbf{F}^{(2)}_{agr} = \left[\begin{array}{cc|cc|cc|cc|cc} 0 & 0 & 0 & 0 & 0 & 0 & 0 & 0 & 0 & 0 \end{array}\right]_{6\times60} \tag{42}$$

For the actuation mode (3) corresponding block matrices have the form

$$\mathbf{A}^{(3)}_{agr} = \left[\begin{array}{cc|cc|cc|cc|cc} 0 & \mathbf{\Lambda}^r_* & -\mathbf{\Lambda}^r_* & 0 & 0 & 0 & 0 & 0 & 0 & 0 \\ \hline 0 & 0 & 0 & \mathbf{\Lambda}^r_* & -\mathbf{\Lambda}^r_* & 0 & 0 & 0 & 0 & 0 \\ \hline 0 & 0 & 0 & 0 & 0 & \mathbf{\Lambda}^r_* & -\mathbf{\Lambda}^r_* & 0 & 0 & 0 \\ 0 & 0 & 0 & 0 & 0 & \mathbf{I} & 0 & 0 & -\mathbf{I} & 0 \\ \hline 0 & 0 & 0 & 0 & 0 & 0 & 0 & \mathbf{\Lambda}^r_* & 0 & 0 \\ \hline \mathbf{\Lambda}^r_* & 0 & 0 & 0 & 0 & 0 & 0 & 0 & 0 & 0 \end{array}\right]_{31\times60} \tag{43}$$

$$\mathbf{B}^{(3)}_{agr} = \left[\begin{array}{cc|cc|cc|cc|cc} 0 & \mathbf{\Lambda}^r_* & \mathbf{\Lambda}^r_* & 0 & 0 & 0 & 0 & 0 & 0 & 0 \\ 0 & \mathbf{\Lambda}^p_* & 0 & 0 & 0 & 0 & 0 & 0 & 0 & 0 \\ 0 & 0 & \mathbf{\Lambda}^p_* & 0 & 0 & 0 & 0 & 0 & 0 & 0 \\ \hline 0 & 0 & 0 & \mathbf{\Lambda}^r_* & \mathbf{\Lambda}^r_* & 0 & 0 & 0 & 0 & 0 \\ 0 & 0 & 0 & \mathbf{\Lambda}^p_* & 0 & 0 & 0 & 0 & 0 & 0 \\ 0 & 0 & 0 & 0 & \mathbf{\Lambda}^p_* & 0 & 0 & 0 & 0 & 0 \\ \hline 0 & 0 & 0 & 0 & 0 & \mathbf{\Lambda}^r_* & \mathbf{\Lambda}^r_* & 0 & \mathbf{\Lambda}^r_* & 0 \\ 0 & 0 & 0 & 0 & 0 & \mathbf{\Lambda}^p_* & 0 & 0 & \mathbf{\Lambda}^p_* & 0 \\ 0 & 0 & 0 & 0 & 0 & 0 & \mathbf{\Lambda}^p_* & 0 & 0 & 0 \\ \hline \mathbf{\Lambda}^p_* & 0 & 0 & 0 & 0 & 0 & 0 & 0 & 0 & 0 \end{array}\right]_{22\times60} \tag{44}$$

$$\mathbf{C}^{(3)}_{agr} = \left[\begin{array}{cc|cc|cc|cc|cc} 0 & 0 & 0 & 0 & 0 & 0 & 0 & -\mathbf{\Lambda}^e_* & 0 & 0 \end{array}\right]_{1\times60} \tag{45}$$

$$\mathbf{D}^{(3)}_{agr} = \left[\begin{array}{cc|cc|cc|cc|cc} K_e\mathbf{\Lambda}^e_* & 0 & 0 & 0 & 0 & 0 & 0 & -K_e\mathbf{\Lambda}^e_* & 0 & 0 \end{array}\right]_{1\times60} \tag{46}$$

$$\mathbf{E}^{(3)}_{agr} = \left[\begin{array}{cc|cc|cc|cc|cc} 0 & 0 & 0 & 0 & 0 & 0 & 0 & 0 & 0 & \mathbf{I} \end{array}\right]_{6\times60} . \tag{47}$$

$$\mathbf{F}^{(3)}_{agr} = \left[\begin{array}{cc|cc|cc|cc|cc} 0 & 0 & 0 & 0 & 0 & 0 & 0 & 0 & 0 & 0 \end{array}\right]_{6\times60} \tag{48}$$

This system can be also transformed to the form (25), where

$$\mathbf{K}_{agr} = \begin{bmatrix} \mathbf{K}_{links} \\ \mathbf{A}_{agr} \\ \mathbf{0}_{22\times60} \\ \mathbf{D}_{agr} \end{bmatrix}_{114\times60} ; \quad \mathbf{S}_{agr} = \begin{bmatrix} -\mathbf{I}_{60\times60} \\ \mathbf{0}_{31\times60} \\ \mathbf{B}_{agr} \\ \mathbf{C}_{agr} \end{bmatrix}_{114\times60} \tag{49}$$

Further, after separating the node variables $\{\Delta\mathbf{t}_i\}$ in two groups corresponding to the internal nodes $\Delta\mathbf{t}_m$ and to the end effector node $\Delta\mathbf{t}_e$ one can compute the desired stiffness ma-

trices for all manipulator legs that will be further denoted as $\mathbf{K}_C^{(1)}, \mathbf{K}_C^{(2)}, \mathbf{K}_C^{(3)}$.

For the entire manipulator, which is composed of three legs (with relevant actuation modes) and the moving platform, the aggregated stiffness model o is presented as follows

$$\begin{bmatrix} -\mathbf{I}_{18\times18} & \mathbf{K}_{platf} \\ \mathbf{B}_{agr} & \mathbf{0}_{3\times24} \\ \mathbf{C}_{agr} & \mathbf{D}_{agr} \\ \mathbf{0}_{6\times18} & \mathbf{F}_{agr} \end{bmatrix}_{42\times42} \cdot \begin{bmatrix} \mathbf{W}_{agr} \\ \Delta\mathbf{t}_{agr} \end{bmatrix}_{42\times1} = \begin{bmatrix} \mathbf{0}_{36\times1} \\ \mathbf{W}_e \end{bmatrix}_{42\times1} \tag{50}$$

where

$$\mathbf{K}_{platf} = \begin{bmatrix} \mathbf{K}_{11}^{(1e)} & 0 & 0 & \mathbf{K}_{12}^{(1e)} \\ 0 & \mathbf{K}_{11}^{(2e)} & 0 & \mathbf{K}_{12}^{(2e)} \\ 0 & 0 & \mathbf{K}_{11}^{(3e)} & \mathbf{K}_{12}^{(3e)} \end{bmatrix}_{18\times24}$$

$$\mathbf{B}_{agr} = \begin{bmatrix} \mathbf{\Lambda}_*^p & 0 & 0 \\ 0 & \mathbf{\Lambda}_*^p & 0 \\ 0 & 0 & \mathbf{\Lambda}_*^p \end{bmatrix}_{3\times18} \qquad \mathbf{C}_{agr} = \begin{bmatrix} -\mathbf{\Lambda}_*^r & 0 & 0 \\ 0 & -\mathbf{\Lambda}_*^r & 0 \\ 0 & 0 & -\mathbf{\Lambda}_*^r \end{bmatrix}_{15\times18}$$

$$\mathbf{D}_{agr} = \begin{bmatrix} \mathbf{\Lambda}_*^r\mathbf{K}_C^{(1)} & 0 & 0 & 0 \\ 0 & \mathbf{\Lambda}_*^r\mathbf{K}_C^{(2)} & 0 & 0 \\ 0 & 0 & \mathbf{\Lambda}_*^r\mathbf{K}_C^{(3)} & 0 \end{bmatrix}_{15\times24}$$

$$\mathbf{F}_{agr} = \begin{bmatrix} \mathbf{K}_{21}^{(1e)} & \mathbf{K}_{21}^{(2e)} & \mathbf{K}_{21}^{(3e)} & \sum_{i=1}^{3}\mathbf{K}_{22}^{(ie)} \end{bmatrix}_{6\times24}$$

For computational convenience, this system can be also converted into the form (25), where

$$\mathbf{K}_{agr} = \begin{bmatrix} \mathbf{K}_{platf} \\ \mathbf{0}_{3\times24} \\ \mathbf{D}_{agr} \end{bmatrix}_{36\times24} ; \quad \mathbf{S}_{agr} = \begin{bmatrix} -\mathbf{I}_{18\times18} \\ \mathbf{B}_{agr} \\ \mathbf{C}_{agr} \end{bmatrix}_{36\times18} \tag{51}$$

Further, after separating the node variables $\{\Delta\mathbf{t}_i\}$ in two groups corresponding internal nodes $\Delta\mathbf{t}_m$ and to the end effector $\Delta\mathbf{t}_e$ one can get the linear systems allowing us to compute the desired stiffness matrix for the entire manipulator. This matrix for different configuration and actuation modes is analyzed in following section.

TABLE II. COMPLIANCE ERRORS FOR DIFFERENT ACTUATION MODES OF NAVARO MANIPULATOR

Actuation mode	Translational errors mm/100N	Rotational errors deg/100Nm
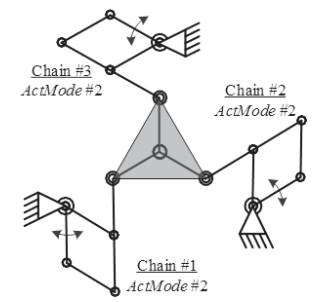	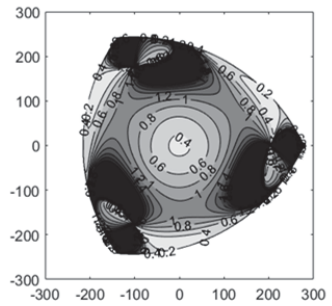	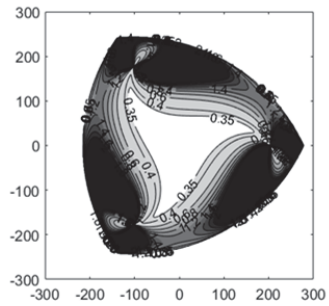
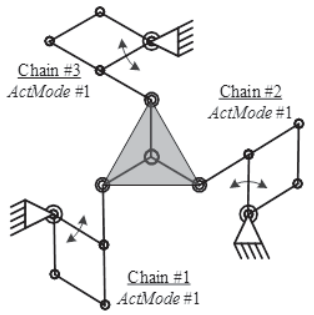	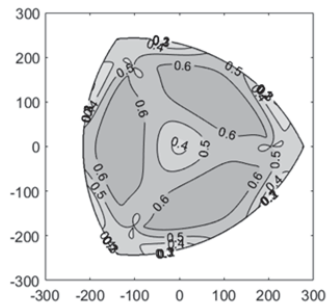	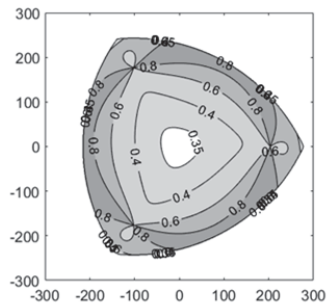
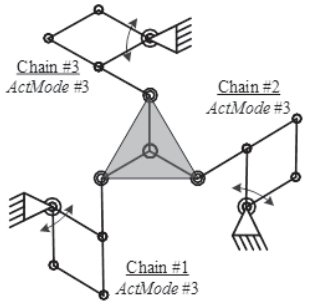	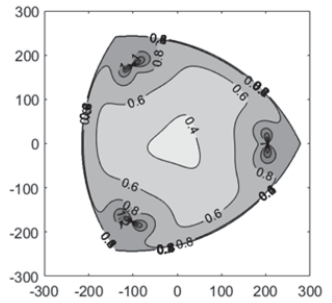	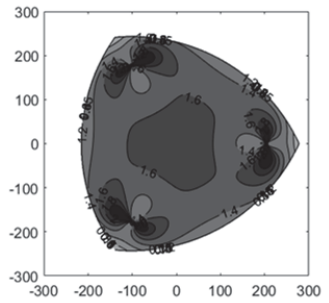

VI. Analysis of Stiffness Behavior

To evaluate the manipulator resistance with respect to the external wrench applied to the end-effector, let us estimate the maximum compliance errors corresponding to the force/torque of the limited magnitude [30]. It allows us to use the singular value decomposition of relevant blocks of the Cartesian compliance matrix $\mathbf{K}_C^{-1}$.

Computational results for different actuation modes are presented in Table II, which shows distribution of the maximum translational [mm] and rotational [deg] deflections within the manipulator workspace. It was assumed that the end-effector is subject to the external loadings of the magnitude 100 N and 100 Nm respectively. As follows from the obtained results, the second actuation mode ensures better stiffness properties for almost all configurations (excluding those close to the singular ones) comparing to the first actuation mode. For instance, for the second actuation mode, the translational compliance error within the circle of 200mm diameter can reach 0.95 mm while for the first actuation mode it is less than 0.65 mm. The third actuation mode provides the highest positioning accuracy in the middle of workspace and achieves for the circle of 200mm diameter accuracy about 0.51 mm. From another side its orientation errors for the same circle about 1.75 deg while the second actuation mode ensures accuracy about 0.40 deg for the same applied external moment.

VII. Conclusions

The paper presents the stiffness analysis for the NaVaRo robot, a three-degree-of-freedom planar parallel manipulator with variable actuation schemes. It also contains new scientific results dealing with extension of the classical MSA technique for the case of complex open-loop and closed-loop manipulators. The proposed approach produces the Cartesian stiffness matrices and presents the manipulator stiffness model as a set of conventional equations describing the link elasticities that are supplemented by a set of constraints describing connections between links. The main advantage is computational simplicity that straightforwardly aggregates the stiffness model equations avoiding traditional column/row merging procedures of the conventional MSA.

Acknowledgments

The work presented in this paper was supported by the grant of Russian Science Foundation №17-19-01740

References

[1] A. Klimchik, A. Ambiehl, S. Garnier, B. Furet, and A. Pashkevich, "Efficiency evaluation of robots in machining applications using industrial performance measure," *Robotics and Computer-Integrated Manufacturing,* vol. 48, pp. 12-29, 12// 2017.

[2] R. Rossi, L. Fossali, A. Novazzi, L. Bascetta, and P. Rocco, "Implicit force control for an industrial robot based on stiffness estimation and compensation during motion," in *2016 IEEE International Conference on Robotics and Automation (ICRA)*, 2016, pp. 1138-1145.

[3] A. Klimchik, D. Bondarenko, A. Pashkevich, S. Briot, and B. Furet, "Compliance Error Compensation in Robotic-Based Milling," in *Informatics in Control, Automation and Robotics*, vol. 283, J.-L. Ferrier, A. Bernard, O. Gusikhin, and K. Madani, Eds. (Lecture Notes in Electrical Engineering: Springer International Publishing, 2014, pp. 197-216.

[4] J. Belchior, M. Guillo, E. Courteille, P. Maurine, L. Leotoing, and D. Guines, "Off-line compensation of the tool path deviations on robotic machining: Application to incremental sheet forming," *Robotics and Computer-Integrated Manufacturing,* vol. 29, no. 4, pp. 58-69, 8// 2013.

[5] A. Pashkevich, A. Klimchik, and D. Chablat, "Enhanced stiffness modeling of manipulators with passive joints," *Mechanism and machine theory,* vol. 46, no. 5, pp. 662-679, 2011.

[6] S. J. Yan, S. K. Ong, and A. Y. C. Nee, "Stiffness analysis of parallelogram-type parallel manipulators using a strain energy method," *Robotics and Computer-Integrated Manufacturing,* vol. 37, pp. 13-22, 2016/02/01/ 2016.

[7] Y. Y. Wang, T. Huang, X. M. Zhao, J. P. Mei, D. G. Chetwynd, and S. J. Hu, "Finite Element Analysis and Comparison of Two Hybrid Robots-the Tricept and the TriVariant," in *Intelligent Robots and Systems, 2006 IEEE/RSJ International Conference on*, 2006, pp. 490-495.

[8] A. Klimchik, A. Pashkevich, and D. Chablat, "CAD-based approach for identification of elasto-static parameters of robotic manipulators," *Finite Elements in Analysis and Design,* vol. 75, no. 0, pp. 19-30, 11/1/ 2013.

[9] K. Nagai and Z. Liu, "A systematic approach to stiffness analysis of parallel mechanisms," in *Robotics and Automation, 2008. ICRA 2008. IEEE International Conference on*, 2008, pp. 1543-1548: IEEE.

[10] S. Marie, E. Courteille, and P. Maurine, "Elasto-geometrical modeling and calibration of robot manipulators: Application to machining and forming applications," *Mechanism and Machine Theory,* vol. 69, no. 0, pp. 13-43, 11// 2013.

[11] D. Deblaise, X. Hernot, and P. Maurine, "A systematic analytical method for PKM stiffness matrix calculation," in *IEEE International Conference on Robotics and Automation (ICRA 2006)*, 2006, pp. 4213-4219: IEEE.

[12] A. Klimchik, A. Pashkevich, S. Caro, and D. Chablat, "Stiffness matrix of manipulators with passive joints: computational aspects," *Robotics, IEEE Transactions on,* vol. 28, no. 4, pp. 955-958, 2012.

[13] C. Quennouelle and C. m. Gosselin, "Instantaneous kinemato-static model of planar compliant parallel mechanisms," in *ASME 2008 International Design Engineering Technical Conferences and Computers and Information in Engineering Conference*, 2008, pp. 163-173: American Society of Mechanical Engineers.

[14] C. Gosselin and D. Zhang, "Stiffness analysis of parallel mechanisms using a lumped model," *International Journal of Robotics and Automation,* vol. 17, no. 1, pp. 17-27, 2002.

[15] A. Pashkevich, A. Klimchik, S. Caro, and D. Chablat, "Cartesian stiffness matrix of manipulators with passive joints: Analytical approach," in *Intelligent Robots and Systems (IROS), 2011 IEEE/RSJ International Conference on*, 2011, pp. 4034-4041.

[16] R. S. Gonçalves, G. Carbone, J. C. M. Carvalho, and M. Ceccarelli, "A comparison of stiffness analysis methods for robotic systems," *International journal of mechanics and control,* vol. 17, no. 2, pp. 35-58, 2016.

[17] H. Liu, T. Huang, D. G. Chetwynd, and A. Kecskeméthy, "Stiffness Modeling of Parallel Mechanisms at Limb and Joint/Link Levels," *IEEE Transactions on Robotics,* vol. 33, no. 3, pp. 734-741, 2017.

[18] J. K. Salisbury, "Active stiffness control of a manipulator in Cartesian coordinates," in *Decision and Control including the Symposium on Adaptive Processes, 1980 19th IEEE Conference on*, 1980, vol. 19, pp. 95-100: IEEE.

[19] C. Gosselin, "Stiffness mapping for parallel manipulators," *Robotics and Automation, IEEE Transactions on,* vol. 6, no. 3, pp. 377-382, 1990.

[20] A. Cammarata, "Unified formulation for the stiffness analysis of spatial mechanisms," *Mechanism and Machine Theory,* vol. 105, pp. 272-284, 2016/11/01/ 2016.

[21] T. Detert and B. Corves, "Extended Procedure for Stiffness Modeling Based on the Matrix Structure Analysis," in *New Advances in Mechanisms, Mechanical Transmissions and Robotics: Proceedings of The International Conference Robotics*

'16, B. Corves, E.-C. Lovasz, M. Hüsing, I. Maniu, and C. Gruescu, Eds. Cham: Springer International Publishing, 2017, pp. 299-310.

[22] S. Shi *et al.*, "Static stiffness modelling of EAST articulated maintenance arm using matrix structural analysis method," *Fusion Engineering and Design,* 2017/05/23/ 2017.

[23] S. Mousavi, V. Gagnol, B. C. Bouzgarrou, and P. Ray, "Model-Based Stability Prediction of a Machining Robot," in *New Advances in Mechanisms, Mechanical Transmissions and Robotics: Proceedings of The Joint International Conference of the XII International Conference on Mechanisms and Mechanical Transmissions (MTM) and the XXIII International Conference on Robotics (Robotics '16)*, B. Corves, E.-C. Lovasz, M. Hüsing, I. Maniu, and C. Gruescu, Eds. Cham: Springer International Publishing, 2017, pp. 379-387.

[24] H. Azulay, M. Mahmoodi, R. Zhao, J. K. Mills, and B. Benhabib, "Comparative analysis of a new 3×PPRS parallel kinematic mechanism," *Robotics and Computer-Integrated Manufacturing,* vol. 30, no. 4, pp. 369-378, 2014/08/01/ 2014.

[25] S. Caro, D. Chablat, and Y. Hu, "Algorithm for the Actuation Mode Selection of the Parallel Manipulator NAVARO," no. 46377, p. V05BT08A063, 2014.

[26] A. Pashkevich, A. Klimchik, D. Chablat, and P. Wenger, "Accuracy improvement for stiffness modeling of parallel manipulators," in *42nd CIRP Conference on Manufacturing Systems*, Grenoble, 2009, p. 8.

[27] A. Klimchik, "Enhanced stiffness modeling of serial and parallel manipulators for robotic-based processing of high performance materials," Ecole Centrale de Nantes, 2011.

[28] A. Klimchik, D. Chablat, and A. Pashkevich, "Advancement of MSA-Technique for Stiffness Modeling of Serial and Parallel Robotic Manipulators," Cham, 2019, pp. 355-362: Springer International Publishing.

[29] A. Klimchik, A. Pashkevich, and D. Chablat, "MSA Technique for Stiffness Modeling of Manipulators with Complex and Hybrid Structures," in *12TH IFAC SYMPOSIUM ON ROBOT CONTROL - SYROCO 2018*, Budapest, Hungary, 2018.

[30] A. Klimchik and A. Pashkevich, "Serial vs. quasi-serial manipulators: Comparison analysis of elasto-static behaviors," *Mechanism and Machine Theory,* vol. 107, pp. 46-70, 1// 2017.